American Mineralogist, Volume 84, pages 1661–1673, 1999

A new complex sheet of uranyl polyhedra in the structure of wölsendorfite

PETER C. BURNS*

Department of Civil Engineering and Geological Sciences, University of Notre Dame, Notre Dame, Indiana 46556-0767, U.S.A.

ABSTRACT

The structure of wölsendorfite, $Pb_{6.16}Ba_{0.36}[(UO_2)_{14}O_{19}(OH)_4](H_2O)_{12}$, $Z = 8$, orthorhombic, $a = 14.131(1)$, $b = 13.885(1)$, $c = 55.969(4)$ Å, $V = 10{,}982$ Å^3, space group *Cmcm*, was solved by direct methods and refined by full-matrix least-squares techniques to an agreement factor (R) of 6.4% and a goodness-of-fit (S) of 1.13 using 6215 unique observed reflections ($|F_o| \geq 4\sigma_F$) collected with Mo$K\alpha$ X-radiation and a CCD (charge-coupled device) detector. The structure contains eight unique U^{6+} positions, each of which is part of a nearly linear $(UO_2)^{2+}$ uranyl ion. The uranyl ions (Ur) are further coordinated by four or five anions (ϕ) arranged at the equatorial corners of square and pentagonal bipyramids, respectively. The structure contains two unique $Ur\phi_4$ square bipyramids and six unique $Ur\phi_5$ pentagonal bipyramids that link by the sharing of equatorial corners and edges to form infinite sheets that are parallel to (100). The sheets have a primitive repeat distance of $c = 55.969$ Å, and are by far the most complex sheet of uranyl polyhedra yet observed. The interlayer between the uranyl sheets contains Pb^{2+} and Ba cations, as well as H_2O groups that are either bonded to the interlayer cations or are held in the structure by H bonding only. There are eight unique cation positions in the interlayer that are coordinated by six to ten anions.

The structure of wölsendorfite is remarkable both in the complexity of the sheets of uranyl polyhedra and the connectivity of the interlayer. By using the sheet anion-topology approach, it is shown that the wölsendorfite sheet is composed of slabs of the simpler α-U_3O_8 and β-U_3O_8-type sheets. It is possible that many as yet unknown complex sheets of uranyl polyhedra exist that are based upon anion topologies that are combinations of slabs of simpler topologies, but it is currently not possible to distinguish which of these may be energetically favorable.

INTRODUCTION

Approximately 200 minerals contain U^{6+} as a necessary structural constituent (Fleischer and Mandarino 1995), and these minerals are significant components of the oxidized portions of U deposits (Frondel 1958; Finch and Ewing 1992). Uranyl minerals are currently receiving considerable attention because of their significance to the environment (e.g., Burns 1998a, 1998b, 1998c, 1997; Burns et al. 1997a, 1997b, 1997c; Finch et al. 1992, 1996, 1998; Finch and Ewing 1992; Miller et al. 1996; Murakami et al. 1997; Sowder et al. 1996; Vochten et al. 1995, 1997). Uranyl minerals are present in the mill tailings that result from the mining of U and are precipitated in soils that are contaminated with actinide elements. Uranyl minerals will be the dominant products of alteration of spent nuclear fuel in a geological repository if the conditions are oxidizing and the fuel comes in contact with water, as is likely to occur at the proposed repository at Yucca Mountain, Nevada (Finn et al. 1996; Wronkiewicz et al. 1996). Uranyl minerals may impact upon the mobility of various radionuclides under repository conditions by incorporating them directly into their crystal structures as they grow (Burns et al. 1997b) or by the exchange of ions between earlier-formed crystals and radionuclide-bearing solutions (Burns 1999).

Despite the obvious importance of uranyl minerals, and the considerable attention that they have garnered, our understanding of their structures and crystal chemistry lags well behind many other mineral groups. To date, the structures have been determined and refined for only ~60 uranyl minerals, less than 1/3 of the known species. The disparity of structural information is due to experimental difficulties; all are extremely high absorbers of X-rays, many do not form crystals of a size suitable for structure analysis using conventional means, and some suffer from dehydration or other effects that cause the deterioration of crystals.

Uranyl minerals are structurally very complex. The U^{6+} cation invariably occurs as part of a nearly linear $(UO_2)^{2+}$ uranyl ion (Ur) in minerals (Evans 1963; Burns et al. 1997a), which is in turn coordinated by four, five, or six additional anions that are arranged at the equatorial corners of square, pentagonal, and hexagonal bipyramids, respectively. The O atoms of the uranyl ion (O_{Ur}) receive ~1.7 valence units (v.u.) from the bond to the U^{6+} cation, whereas considerably less of the bond-valence requirements of the equatorial ligands are provided by the bond to the U^{6+} cation at the center of the polyhedron. Polymerization of uranyl polyhedra with other uranyl polyhedra,

*E-mail: peter.burns.50@nd.edu

0003-004X/99/0010–1661$05.00

as well as other cation polyhedra of higher bond-valence, is common in mineral structures, as this permits the bonding requirements of the equatorial ligands to be met. The strongly asymmetric distribution of bond valences in the uranyl polyhedra dictates that the structures of uranyl minerals are dominated by sheets of polymerized polyhedra (Burns et al. 1996, 1997a).

An interesting and complex subgroup of uranyl minerals is the lead uranyl oxide hydrates (Table 1). These minerals commonly form due to the oxidation of geologically old uraninite, owing to an abundance of radiogenic Pb. The onset of alteration of uraninite, UO_{2+x}, typically results in the formation of a sequence of lead uranyl oxide hydrates as continued alteration preferentially removes U^{6+} relative to Pb (Frondel 1958). Each structure is based upon complex sheets of edge- and corner-sharing uranyl polyhedra (Fig. 1), with the uranyl ions oriented roughly perpendicular to the sheet, and with Pb^{2+} cations and H_2O groups located in the interlayers between the sheets. The fourmarierite-type sheet also occurs in schoepite (Finch et al. 1996), and the richetite-type sheet occurs in becquerelite (Pagoaga et al. 1987), compreignacite (Burns 1998c), billietite (Pagoaga et al. 1987), and protasite (Pagoaga et al. 1987). The curite-type sheet is not known from another mineral, but it does occur in the structure of the synthetic Sr analogue of curite (Burns and Hill 1999). The sayrite-type sheet was first found in the structure of $K_2[(UO_2)_5O_8](UO_2)_2$ (Kovba 1972), and later in sayrite. The vandendriesscheite-type sheet has not yet been found in another structure, and until the current work it was the most complex sheet of uranyl polyhedra known.

Wölsendorfite was first discovered in Wölsendorf, Bavaria, Germany (Protas 1957) and has since been reported from several localities where it occurs in the oxidized portions of U deposits. The currently accepted formula is $(Pb,Ba,Ca)U_2O_7 \cdot 2H_2O$ (Fleischer and Mandarino 1995). Ba-rich wölsendorfite contain-

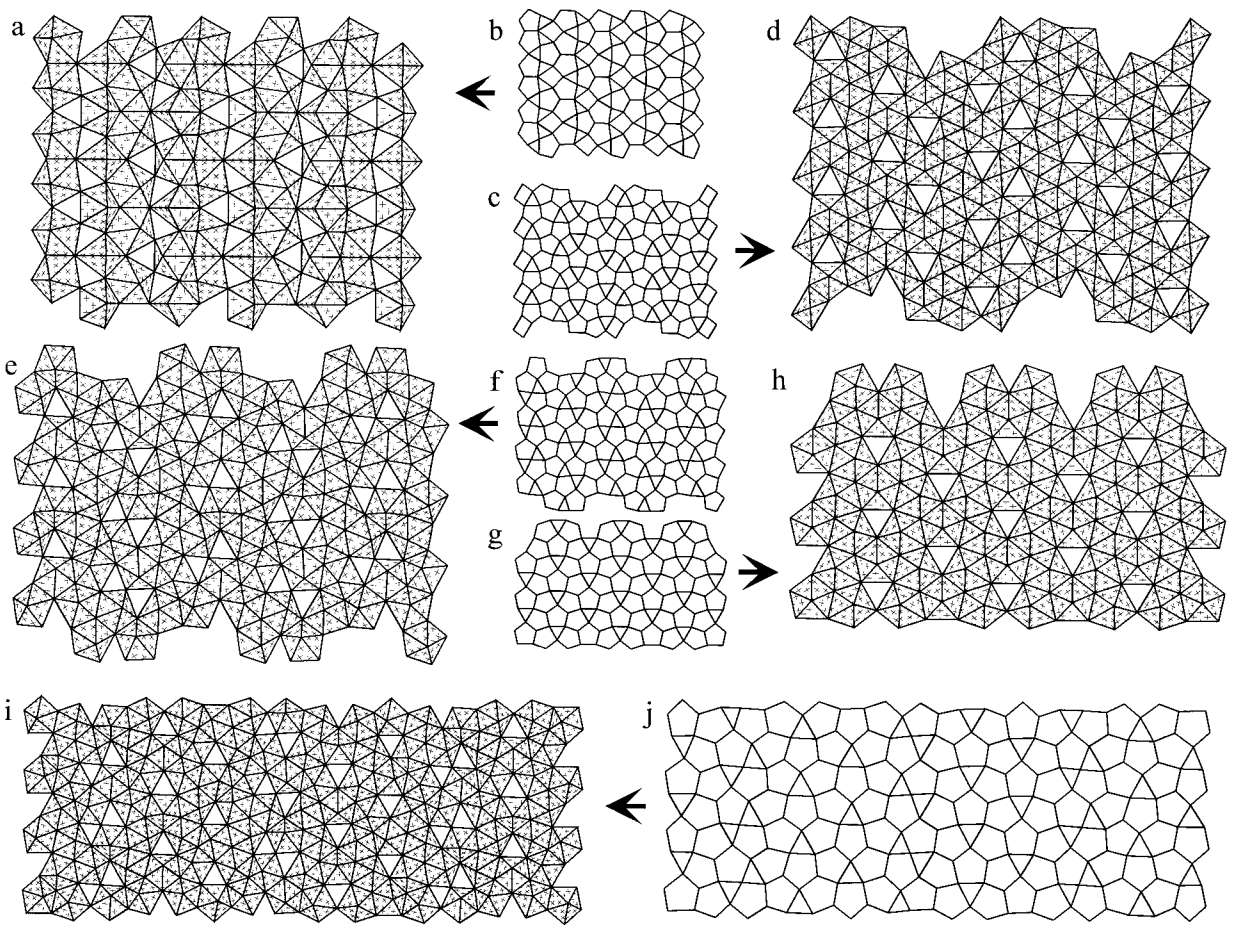

FIGURE 1. Polyhedral representations and anion topologies of the sheets that occur in lead uranyl oxide hydrate minerals. (**a**) curite, (**b**) curite anion-topology, (**c**) sayrite anion-topology, (**d**) sayrite, (**e**) fourmarietite, (**f**) fourmarierite anion-topology, (**g**) richetite anion-topology, (**h**) richetite, (**i**) vandendriesscheite, (**j**) vandendriesscheite anion-topology. The sheet anion-topologies were derived using the method of Burns et al. (1996). Uranyl polyhedra are shaded with crosses.

TABLE 1. The chemistries of lead uranyl oxide hydrates

	Pb:U	Sheet composition	Ref.
wölsendorfite	1:2.15	$[(UO_2)_{14}O_{19}(OH)_4]$	*
sayrite	1:2.5	$[(UO_2)_5O_6(OH)_2]$	†
curite	1:2.67	$[(UO_2)_8O_8(OH)_6]$	‡
fourmarierite	1:4.0	$[(UO_2)_4O_3(OH)_4]$	§
richetite	1:4.15	$[(UO_2)_{18}O_{18}(OH)_{12}]$	||
vandendriesscheite	1:6.36	$[(UO_2)_{10}O_6(OH)_{11}]$	#

* This study.
† Piret et al. (1983).
‡ Taylor et al. (1981).
§ Piret (1985).
|| Burns (1998a).
Burns (1997).

TABLE 2. Miscellaneous information pertaining to the structure determination of wölsendorfite

a (Å)	14.131(1)	Crystal size (mm)	0.20 × 0.10
b (Å)	13.885(1)		× 0.01
c (Å)	55.969(4)	Total ref.	25,370
V (Å^3)	10,982	Unique ref.	7026
Space group	*Cmcm*	R_{int} (%)	7.0
F(000)	18,762	Unique $\|F_o\| \geq 4\sigma_F$	6215
m (mm^{-1})	60.30	Final *R** (%)	6.4
D_{calc} (g/cm^3)	6.888	*S*†	1.13

Unit-cell contents: $8\{Pb_{6.16}Ba_{0.36}[(UO_2)_{14}O_{19}(OH)_4](H_2O)_{12}\}$

* $R = \Sigma(|F_o|-|F_c|)/\Sigma|F_o|$.
† $S = [\Sigma w(|F_o|-|F_c|)^2/(m-n)]^{1/2}$, for *m* observations and *n* parameters.

ing 3.27 wt% BaO and 0.09 wt% CaO was found in Greenland by Beddoe-Stephens and Secher (1982), and Ca-rich wölsendorfite containing 3.24 wt% CaO but no reported BaO is known from a U-Mo ore deposit in Russia (Belov and Federov 1974). The synthetic Ca- and Ba-free endmember has been reported by Vochten and Haverbeke (1990). Toussaint (1961) provided a partial structure solution for a crystal of wölsendorfite from Shinkolobwe, Democratic Republic of Congo, but was only able to propose the positions of the U atoms based upon a sub-cell. He reported the unit-cell dimensions $a = 11.9$, $b = 6.99$, $c = 6.85$ Å, and noted that the X-ray data indicated the true *b* unit-cell dimension was probably double that reported, and the *c* unit-cell dimension was probably four times the value reported.

The recent introduction of CCD-based detectors for X-rays to mineral structure analysis (Burns 1998d) has greatly facilitated the study of the structures of uranyl minerals, as it is now possible to study very small crystals [i.e., less than $(10\ \mu m)^3$], and crystals with very long primitive unit-cell axes using sealed-tube X-ray sources. This paper presents the full solution of the structure of wölsendorfite using a CCD-based diffractometer.

EXPERIMENTAL METHODS

X-ray data

The specimen provided by the Canadian Museum of Nature is from Shinkolobwe, Democratic Republic of Congo. It contains several tabular crystals of wölsendorfite that exhibited uniform optical properties and sharp extinction between crossed polarizers. A crystal with approximate dimensions 0.20 × 0.10 × 0.01 mm was selected for XRD, and was mounted on a Bruker PLATFORM 3-circle goniometer equipped with a 1K SMART CCD (charge-coupled device) detector.

Preliminary examination revealed a primitive unit-cell axis ~56 Å long. The crystal-to-detector distance was set at 15 cm to obtain excellent resolution of the long axis. The data was collected using monochromatic Mo*K*α X-radiation and frame widths of 0.3° in ω, with 120 s used to acquire each frame. Three different detector settings ($2\theta = 12.0, 30.0, 50.0°$) were used so as to obtain complete coverage to ~57° 2θ. A total of 6588 frames of data were collected, providing a complete sphere of three-dimensional data. The peaks were sharp with smooth profiles, indicating that substantial radiation damage has not occurred. Several hundred frames of data were analyzed to locate diffraction maxima; all peaks found were consistent with a *C*-centered unit cell with the dimensions $a = 14.131(1)$, $b = 13.885(1)$, $c = 55.969(4)$ Å. The long primitive *c* dimension was verified by collection of zone-axis frames. The *C*-centered cell has a strong primitive sub-cell with dimensions $a = 12.01$, $b = 7.101$, $c = 6.935$ Å, in agreement with the sub-cell found by Toussaint (1961). However, the CCD detector provides ample sensitivity and resolution to resolve the true *C*-centered unit cell. The final unit-cell dimensions were refined (Table 2) using least-squares techniques. Data were collected for $3° \leq 2\theta \leq 56.7°$ in approximately 229 hours; comparison of the intensities of equivalent reflections collected at different times during the data collection showed no evidence of significant decay. The three-dimensional data were reduced and corrected for Lorentz, polarization, and background effects using the Bruker program SAINT. An empirical absorption-correction was done based upon 3999 intense reflections with five or more equivalents. The crystal was modeled as a (100) plate; reflections with a plate-glancing angle of less than 3° were discarded from the data set, and the correction lowered $R_{azimuthal}$ from 35.3 to 6.8%. A total of 53 816 reflections was collected, of which 4080 were omitted because of a plate-glancing angle less than 3°. Systematic absences indicated that the lattice is *C*-centered; of the collected reflections, 25 370 were consistent with the *C*-centered lattice. Merging of equivalent reflections gave 7026 unique reflections ($R_{INT} = 7.0\%$) with 6215 classed as observed ($|F_o| \geq 4\sigma_F$).

Chemical analysis

The same specimen used for XRD was mounted, polished, and coated with carbon. Chemical analysis was done in wavelength-dispersion (WD) mode on a JEOL 733 electron microprobe using Tracor Northern 5500 and 5600 automation. Data reduction was done with a conventional PAP routine. The operating voltage was 15 kV, and the beam current was 0.20 μA. Data for all elements in the sample were collected for 25 s or 0.50% precision, whichever was attained first. A 100 s energy-dispersion scan indicated no elements with *Z* greater than 8, other than those reported here. The elements Na, K, Rb, Cs, Ca, and Sr were sought in WD scans, but were not detected. Standards used for the electron-microprobe analysis were: benitoite (Ba*L*α), crocoite (Pb*M*α), and brannerite (U*M*β). H_2O was calculated by stoichiometry from the results of the crystal-structure analysis. The results were (wt%): BaO = 0.99, UO_3 = 72.23, PbO = 24.57, H_2O = 3.90, total = 101.69.

STRUCTURE SOLUTION AND REFINEMENT

Scattering curves for neutral atoms, together with anomalous dispersion corrections, were taken from *International Tables for X-Ray Crystallography, Vol. IV* (Ibers and Hamilton 1974). The Bruker SHELXTL Version 5 system of programs was used for the determination and refinement of the crystal structure.

Systematic absences and reflection statistics indicated the space group *Cmcm* (no. 63), with verification provided by the successful solution and refinement of the structure. The structure was solved by direct methods, and the initial model included the positions of the U atoms and some of the Pb atoms. Additional Pb sites and the anions were located in successive difference-Fourier maps that were calculated after refinement of the model. Following refinement of the atomic positional parameters and isotropic-displacement parameters for all atoms, occupancy factors were included for each Pb site. The agreement factor (*R*) at this stage of the refinement was 10.9% for observed reflections. The site-occupancy factors for the Pb1 through Pb5 sites remained close to 100% occupancy, and were constrained to full occupancy in subsequent cycles of refinement. The occupancy factors for the sites Pb6 through Pb8 refined to values significantly below 100% and were thus included in further cycles of refinement. Consideration of the polyhedral bond-lengths for the Pb sites, and the lack of additional sites in the difference-Fourier maps, indicate that the Ba revealed by the microprobe analysis is probably located at the Pb8 site, and all Ba from the microprobe analysis was subsequently assigned to that site. However, additional scattering was required at the Pb8 site, thus Pb was also included at the site and the occupancy factor was refined. The displacement parameters for the cations were converted to anisotropic forms, and were refined together with the positional parameters for all atoms and a weighting scheme of the structure factors. At this stage in the refinement a peak with height ~11 e/Å^3 was located in the difference-Fourier map ~0.56 Å from the Pb7 site. This site contained too much electron density to correspond to an anion, so it was assumed that the Pb7 site is disordered between two positions, and a new position designated Pb7A was added to the refinement. The occupancy factors of both the Pb7 and Pb7A sites were refined, although the displacement parameter for the Pb7A site was constrained to be isotropic. The final model resulted in an *R* index of 6.4% for 6215 unique observed reflections ($|F_o| \geq 4\sigma_F$) and a goodness-of-fit (*S*) of 1.13. In the final cycle of refinement the average parameter shift/esd was 0.000, and the maximum peaks in the final difference-Fourier maps were 5.74 and –6.12 e/Å^3. The final atomic-positional parameters and anisotropic-displacement parameters are given in Tables 3 and 4, and selected interatomic-distances and angles are given in Table 5. Calculated and observed structure factors are provided in Table 6[1]

[1] For a copy of Table 6, Document AM-99-029 contact the Business Office of the Mineralogical Society of America (see inside front cover of recent issue) for price information. Deposit items may also be available on the American Mineralogist web site (see inside back cover of a current issue for a web address).

TABLE 3. Atomic position parameters and equivalent isotropic-displacement parameters for the structure of wölsendorfite

	x	*y*	*z*	U_{eq}*
U1	0.23236(7)	0.28097(7)	¼	136(2)
U2	0.24043(5)	0.48445(4)	0.07525(1)	99(1)
U3	0.23354(7)	½	0	133(2)
U4	0.26009(5)	0.52736(5)	0.14137(1)	99(1)
U5	0.26058(5)	0.25302(4)	0.10659(1)	101(1)
U6	0.26867(5)	0.50400(5)	0.21281(1)	142(2)
U7	0.24934(5)	0.27115(4)	0.03319(1)	99(1)
U8	0.24787(5)	0.24360(5)	0.18258(1)	127(1)
Pb1	½	0.70072(9)	0.13777(3)	315(3)
Pb2	½	0.3534(1)	–0.00028(2)	322(3)
Pb3	½	0.83007(9)	0.07678(3)	330(3)
Pb4	½	0.08653(9)	0.18238(2)	339(3)
Pb5	½	0.3206(1)	0.07673(2)	472(5)
Pb6	0	0.4681(2)	¼	423(10)
Pb7	½	0.4363(4)	¼	622(15)
Pb7A	½	0.476(4)	¼	548(92)
Pb8	0	0.1683(3)	0.21848(6)	667(16)
O1	0.104(2)	0.305(2)	¼	246(45)
O2	0.246(1)	0.596(1)	0.1043(2)	159(27)
O3	0.368(1)	0.498(1)	0.0708(3)	276(34)
O4	0.360(2)	0.254(1)	¼	234(44)
O5	0.268(1)	0.410(1)	0.1130(3)	238(31)
O6	0.243(1)	0.347(1)	0.2132(2)	215(31)
O7	0.387(1)	0.548(1)	0.1385(3)	258(33)
O8	0.135(1)	0.508(1)	0.1459(3)	320(37)
O9	0.391(2)	0.248(1)	0.1029(4)	492(51)
O10	0.129(2)	0.257(1)	0.1091(4)	478(51)
O11	0.124(2)	0.244(2)	0.0360(4)	554(57)
O12	0.272(2)	0.202(2)	0.1430(4)	510(55)
O13	0.375(2)	0.296(1)	0.0317(3)	441(47)
O14	0.229(1)	0.436(1)	0.0362(3)	296(36)
O15	0.397(2)	0.486(2)	0.2128(4)	530(56)
O16	0.114(1)	0.469(1)	0.0794(3)	284(34)
O17	0.362(3)	½	0	724(104)
O18	0.274(2)	0.584(1)	0.1791(4)	439(47)
O19	0.141(2)	0.524(2)	0.2133(4)	567(59)
O20	0.272(2)	0.159(2)	0.0038(4)	531(55)
O21	0.250(2)	0.318(2)	0.0723(5)	665(70)
O22	0.373(1)	0.221(1)	0.1881(3)	286(34)
O23	0.123(1)	0.267(1)	0.1763(3)	315(37)
O24	0.104(3)	½	0	729(106)
O25	0.298(1)	0.662(1)	0.2221(3)	248(32)
O26	0.265(3)	0.459(3)	¼	701(103)
OH27	0.297(1)	0.393(1)	0.1662(2)	211(29)
OH28	0.292(1)	0.132(1)	0.0555(2)	193(29)
H_2O29	½	0.153(1)	0.2241(4)	208(42)
H_2O30	½	0.889(2)	0.1239(5)	426(65)
H_2O31	½	0.393(2)	0.1692(5)	378(60)
H_2O32	0	0.127(2)	0.0923(4)	301(51)
H_2O33	½	0.143(2)	0.0583(5)	408(62)
H_2O34	½	0.495(2)	0.0343(4)	306(52)
H_2O35	½	0.415(2)	0.1131(6)	605(88)
H_2O36	½	0.210(2)	0.1468(4)	328(55)
H_2O37	½	0.931(3)	0.0404(7)	800(118)
H_2O38	0	0.393(2)	0.2017(5)	411(63)
H_2O39	½	0.172(3)	0.0103(6)	618(90)
H_2O40	½	0.101(1)	0.1067(3)	16(27)

Note: U_{eq}* = U_{eq} Å^2 × 10^4.

RESULTS

Projection of the structure along [010] shows that it contains sheets of uranyl polyhedra parallel to (100), with Pb^{2+} and Ba cations as well as H_2O groups located in the interlayer between the sheets (Fig. 2). The structure of wölsendorfite is therefore consistent with the generalities of other lead uranyl oxide hydrate mineral structures, as well as with the observation that the majority of uranyl mineral structures are based upon sheets of polyhedra of higher bond-valence (Burns et al. 1996).

TABLE 4. Anisotropic-displacement parameters for the cations in the structure of wölsendorfite

	U_{11}*	U_{22}	U_{33}	U_{12}	U_{13}	U_{23}
U1	153(4)	171(4)	85(4)	42(4)	0	0
U2	148(3)	75(3)	73(3)	–21(2)	18(2)	–15(2)
U3	127(4)	86(4)	188(4)	0	0	23(3)
U4	160(3)	78(3)	59(3)	–9(2)	12(2)	–3(2)
U5	121(3)	76(3)	107(3)	–5(2)	3(2)	–1(2)
U6	145(3)	155(3)	124(3)	–9(3)	–11(3)	62(2)
U7	148(3)	81(3)	68(3)	17(2)	–13(2)	–11(2)
U8	208(3)	80(3)	93(3)	24(2)	8(3)	–11(2)
Pb1	251(6)	219(6)	476(8)	0	0	–42(5)
Pb2	375(7)	348(6)	243(6)	0	0	49(5)
Pb3	268(6)	253(6)	469(8)	0	0	–3(5)
Pb4	505(8)	237(6)	274(6)	0	0	24(5)
Pb5	1030(15)	203(6)	182(6)	0	0	4(5)
Pb6	722(23)	260(13)	288(14)	0	0	0
Pb7	1199(38)	157(24)	510(20)	0	0	0
Pb8	1029(36)	609(24)	363(19)	0	0	311(15)

Note: U_{ij}* = U_{ij} Å^2 × 10^4

U coordination

The structure contains eight symmetrically distinct U sites, and each is contained within the sheet of uranyl polyhedra that is parallel to (100) at $x \approx 1/4$ and $3/4$. Consideration of the polyhedral geometries (Table 5) and the bond-valence sums incident upon each of the U sites (Table 7) demonstrates that each site is occupied by U^{6+}. In all cases the U^{6+} cation is strongly bonded to two O atoms, forming approximately linear $(UO_2)^{2+}$ uranyl ions. The U^{6+}-O_{Ur} bond-lengths are all ~1.8 Å, which is consistent with uranyl ions in well-refined structures (Burns et al. 1997a). The uranyl ions are coordinated by four or five additional anions, resulting in $Ur\phi_4$ square bipyramids and $Ur\phi_5$ pentagonal bipyramids, respectively (ϕ: unspecified ligand). Both types of coordination polyhedra are prevalent in uranyl minerals, although pentagonal bipyramids are the most common (Burns et al. 1997a).

The U3 and U5 uranyl ions are coordinated by four O atoms located at the corners of UrO_4 square bipyramids, and have <U^{6+}-O_{eq}> bond-lengths (eq: equatorial) of 2.21 and 2.17 Å, respectively, which can be compared to the <$^{[6]}U^{6+}$-ϕ_{eq}> bond-length of 2.28(5) Å in well-refined structures (Burns et al. 1997a). The remaining uranyl ions are each coordinated by five anions; the U1 uranyl ion is coordinated by five equatorial O atoms, whereas each of the U2, U4, U6, U7, and U8 uranyl ions are coordinated by four equatorial O atoms and one $(OH)^-$ group. The <$^{[7]}U^{6+}$-ϕ_{eq}> bond-lengths range from 2.32 to 2.38 Å, which can be compared to the <$^{[7]}U^{6+}$-ϕ_{eq}> of 2.37(9) Å in numerous well-refined structures (Burns et al. 1997a).

The coordination polyhedron about the U6 position warrants additional comment. The U^{6+}-O_{eq} bond-lengths are in the range 2.17 to 2.29 Å, but the U^{6+}-$(OH)^-_{eq}$ separation is 3.06 Å. However, the $(OH)^-$ group is in the correct position to be regarded as an equatorial ligand of a $Ur\phi_5$ pentagonal bipyramid, and the bond-valence parameters provided by Burns et al. (1997a) indicate that this interaction has 0.14 valence units (v.u.) associated with it. Therefore, although this separation is considerably longer than most U^{6+}-ϕ_{eq} bond-lengths, it is likely that it does correspond to a weak bond. A similar conclusion was drawn for a U^{6+}-ϕ bond of 3.02(7) Å in the structure of billietite by Pagoaga et al. (1987).

TABLE 5. Selected interatomic distances (Å) and angles (°) in the structure of wölsendorfite

U1-O4	1.84(2)	U5-O9	1.86(2)
U1-O1	1.85(2)	U5-O10	1.87(2)
U1-O6,a	2.26(1) ×2	U5-O21	2.13(3)
U1-O25b,c	2.31(2) ×2	U5-O12	2.16(2)
U1-O26	2.52(4)	U5-O2b	2.18(1)
<U1-O_{Ur}>	1.84	U5-O5	2.22(2)
O4-U1-O1	179.0(9)	<U5-O_{Ur}>	1.86
<U1-ϕ_{eq}>	2.33	O9-U5-O10	177.9(9)
		<U5-ϕ_{eq}>	2.17
U2-O16	1.82(2)		
U2-O3	1.83(2)	U6-O19	1.83(3)
U2-O2	2.25(1)	U6-O15	1.83(2)
U2-O14	2.29(2)	U6-O26	2.17(1)
U2-O21	2.32(3)	U6-O18	2.19(2)
U2-OH28d	2.37(1)	U6-O6	2.21(1)
U2-O5	2.38(2)	U6-O25	2.29(2)
<U2-O_{Ur}>	1.82	U6-OH27	3.06(2)
O16-U2-O3	178.8(8)	<U6-O_{Ur}>	1.83
<U2-f_{eq}>	2.32	O19-U6-O15	178.7(9)
		<U6-f_{eq}>	2.38
U3-O17	1.81(4)		
U3-O24	1.83(4)	U7-O13	1.81(2)
U3-O14,e	2.21(2) ×2	U7-O11	1.82(2)
U3-O20d,f	2.22(2) ×2	U7-O21	2.28(3)
<U3-O_{Ur}>	1.82	U7-O20	2.29(2)
O17-U3-O24	180	U7-O20f	2.31(2)
<U3-ϕ_{eq}>	2.21	U7-O14	2.32(2)
		U7-OH28	2.38(1)
U4-O8	1.80(2)	<U7-O_{Ur}>	1.81
U4-O7	1.83(2)	O13-U7-O11	177.5(9)
U4-O18	2.26(2)	<U7-ϕ_{eq}>	2.32
U4-O5	2.27(2)		
U4-O2	2.29(1)	U8-O22	1.82(2)
U4-OH27	2.39(1)	U8-O23	1.82(2)
U4-O12d	2.47(2)	U8-O6	2.24(1)
<U4-O_{Ur}>	1.81	U8-O18b	2.25(2)
O8-U4-O7	177.0(7)	U8-O12	2.31(2)
<U4-ϕ_{eq}>	2.34	U8-OH27	2.37(1)
		U8-O25b	2.57(2)
		<U8-O_{Ur}>	1.82
		O22-U8-O23	178.7(7)
		<U8-ϕ_{eq}>	2.35
Pb1-O10d,g	2.55(2) ×2	Pb5-O9,l	2.35(2) ×2
Pb1-O7,h	2.66(2) ×2	Pb5-H_2O35	2.42(3)
Pb1-H_2O30	2.73(3)	Pb5-H_2O33	2.68(3)
Pb1-H_2O32g	2.75(2)	Pb5-O13,l	3.10(2) ×2
Pb1-O23d,g	2.92(2) ×2	Pb5-O3,l	3.10(2) ×2
<Pb-ϕ>	2.72	<Pb5-ϕ>	2.77
Pb2-H_2O39	2.59(3)	Pb6-O1,m	2.69(2) ×2
Pb2-O13,h	2.64(2) ×2	Pb6-H_2O38,a	2.90(3) ×2
Pb2-H_2O34	2.76(2)	Pb6-H_2O29n,o	2.95(2) ×2
Pb2-O17,i	2.82(3) ×2	Pb6-O19,m,a,p	2.96(2) ×4
Pb2-H_2O34i	2.84(2)	<Pb6-ϕ>	2.89
Pb2-O11f,j	2.98(2) ×2		
<Pb2-ϕ>	2.79	Pb7-O15,l,a,q	2.63(2) ×4
		Pb7-O4,h	3.21(2) ×2
Pb3-H_2O37	2.47(4)	<Pb7-ϕ>	2.82
Pb3-O16d,g	2.52(2) ×2		
Pb3-O10d,g	2.76(2) ×2	Pb8-O25r,s	2.87(2) ×2
Pb3-H_2O30	2.76(3)	Pb8-O15r,s	2.93(2) ×2
Pb3-H_2O32g	2.95(2)	Pb8-O1,m	2.98(2) ×2
Pb3-O11d,g	3.12(2) ×2	Pb8-O23,m	3.23(2) ×2
<Pb3-ϕ>	2.78	<Pb8-ϕ>	3.00
Pb4-H_2O29	2.51(2)		
Pb4-O22,h	2.61(2) ×2		
Pb4-H_2O36	2.63(2)		
Pb4-O19b,k	2.78(2) ×2		
Pb4-H_2O38k	2.90(3)		
Pb4-O8b,k	3.01(2) ×2		
<Pb4-ϕ>	2.76		

Notes: a = x, y, ½-z; b = ½-x, y-½, z; c = ½-x, y-½, ½-z; d = ½-x, y+½, z; e = x, 1-y, z; f = ½-x, ½-y, -z; g = x+½, y+½, z; h = 1-x, y, z; i = 1-x, 1-y, -z; j = x+½, ½-y, -z; k = x+½, y-½, z; l = 1-x, y, z; m = -x, y, z; n = x-½, y+½, z; o = x-½, y+½, ½-z; p = -x, y, ½-z; q = 1-x, y, ½-z; r = ½-x, y-½, z; s = x-½, y-½, z.

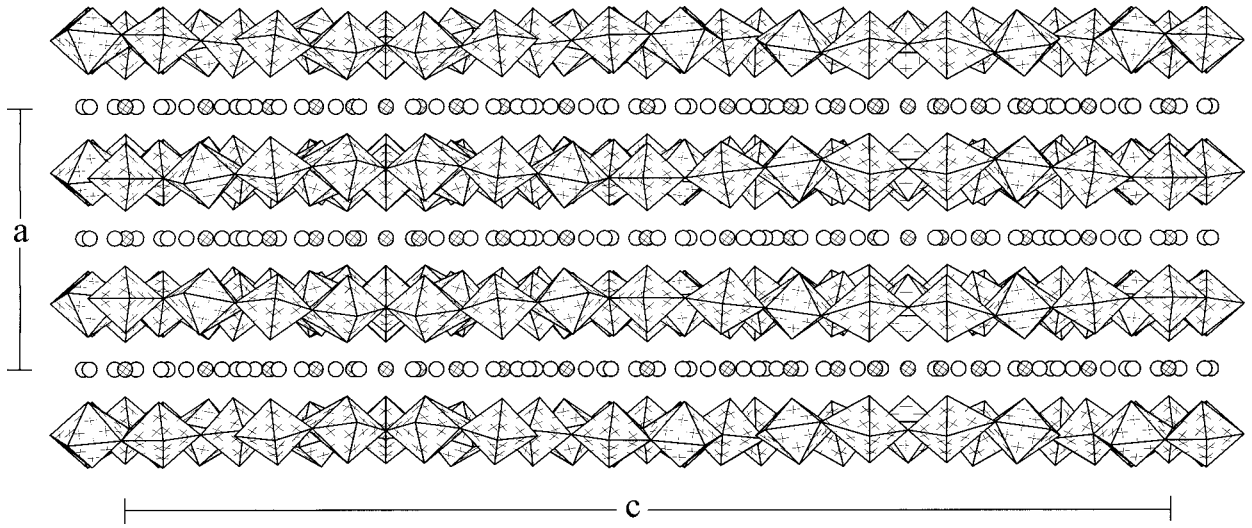

FIGURE 2. Projection of the structure of wölsendorfite along [010]. The uranyl polyhedra are shaded with crosses, Pb^{2+} cations are shown as cross-hatched circles, and H_2O groups are shown as open circles.

TABLE 7. Bond-valence sums* at cation and anion positions in the structure of wölsendorfite.

U1	5.86	Pb1	1.66	O1	1.87	O9	1.96	O17	1.88	O25	1.70	H_2O33	0.22
U2	6.00	Pb2	1.55	O2	2.05	O10	1.89	O18	2.08	O26	1.96	H_2O34	0.31
U3	6.27	Pb3	1.80	O3	1.59	O11	1.72	O19	1.79	OH27	1.18	H_2O35	0.43
U4	6.00	Pb4	1.73	O4	1.55	O12	1.83	O20	1.92	OH28	1.05	H_2O36	0.25
U5	6.27	Pb5	1.98	O5	1.87	O13	1.89	O21	2.06	H_2O29	0.44	H_2O37	0.38
U6	6.06	Pb6	1.27	O6	2.06	O14	1.93	O22	1.81	H_2O30	0.36	H_2O38	0.28
U7	6.09	Pb7	1.00	O7	1.75	O15	1.88	O23	1.72	H_2O31	0.00	H_2O39	0.27
U8	5.94	Pb8	0.77	O8	1.71	O16	1.89	O24	1.52	H_2O32	0.28	H_2O40	0.00

* Calculated using the parameters of Brese and O'Keeffe (1991) for Pb^{2+} and Burns et al. (1997a) for U^{6+}.

Pb coordination

There are eight symmetrically distinct cation sites in the interlayer (excluding H). Of these, the Pb1 through Pb5 sites contain only Pb, and each is fully occupied according to site-scattering refinement. The Pb6 and Pb7 sites are partially occupied, and the latter is disordered over two positions separated by 0.56 Å. The occupancies of the Pb6 and Pb7 sites are 76 and 96%, respectively, according to the results of site-scattering refinement. The Pb8 site contains both Pb and Ba, and all of the Ba indicated by the chemical analysis was assigned to the site. Refinement of the Pb occupancy at the site indicates that it contains ~36% Ba, ~30% Pb, and ~31% vacancy.

The polyhedral geometries (Table 5) and bond-valence sums incident upon the sites (Table 7) are consistent with all Pb present as Pb^{2+}, as is the case for all known Pb uranyl oxide hydrate minerals. The polyhedra are illustrated in Figure 3. Each of the Pb sites is located on the *m* planes at $x = 0, ½$, and the Pb6 and Pb7 sites are at the intersection of two *m* planes. The Pb1 through Pb7 cations are coordinated by O_{Ur} atoms of adjacent sheets, as well as H_2O groups located on the *m* planes in the interlayer at $x = 0, ½$. In addition to O_{Ur} and interlayer H_2O groups, the Pb8 site is coordinated by two O atoms that are equatorial ligands of uranyl polyhedra within the sheets. The Pb1 and Pb5 sites are coordinated by six O_{Ur} atoms and two H_2O groups, the Pb2, Pb3, and Pb4 polyhedra each contain six O_{Ur} atoms and three H_2O groups, and the Pb6 site is coordinated by six O_{Ur} atoms and four H_2O groups. The Pb1 through Pb5 sites have <Pb-ϕ> bond-lengths in the range 2.72 to 2.79 Å, and the <Pb-ϕ> bond-length of the tenfold-coordinated Pb6 is 2.89 Å. The sixfold-coordinated Pb7 site involves shorter bonds, with a <Pb-ϕ> bond-length of 2.49 Å. The Pb8 site has a <Pb-ϕ> bond-length of 3.00 Å, which is in accord with the site containing substantial Ba as well as vacancy.

Polyhedra containing Pb^{2+} are often distorted owing to the presence of a lone pair of electrons on the Pb^{2+} cation. The anions are repelled away from the electron lone-pair, resulting in a one-sided coordination polyhedron. The Pb polyhedra in the interlayer of wölsendorfite (Fig. 3) are fairly irregular, and some are distinctly one-sided, suggesting that the Pb^{2+} cations are lone-pair stereoactive.

Structural formula

Of the eight symmetrically distinct U^{6+} cations, only the U1 site is on a special position, thus the unit cell contains 120 U^{6+} cations. The interlayer contains both Pb and Ba, and site-occupancy refinements have demonstrated that the Pb1 through Pb5 sites are 100% occupied by Pb. The Pb6 and Pb7 sites are partially occupied by Pb, and the Pb8 site contains both Pb and Ba. Each of the interlayer cations are on special positions, thus, according to site-scattering refinement, the unit cell contains

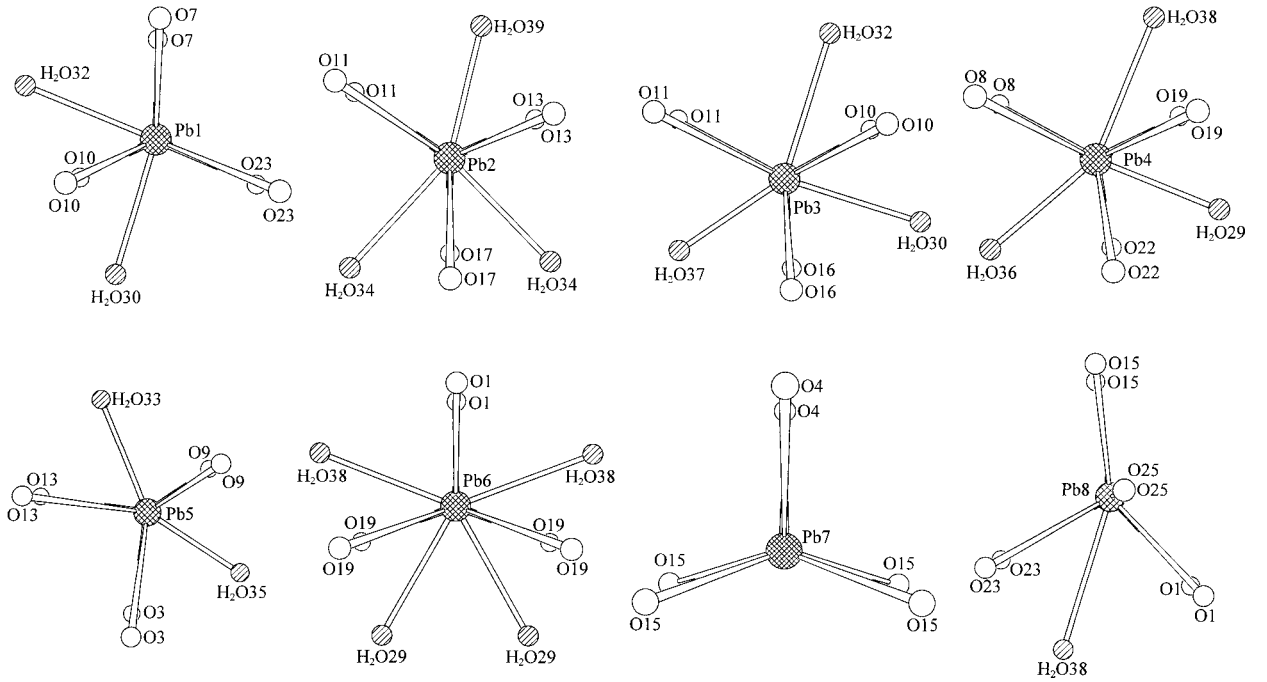

FIGURE 3. The Pb^{2+} polyhedra that occur in the interlayer of wölsendorfite. Each polyhedron is shown projected along [100].

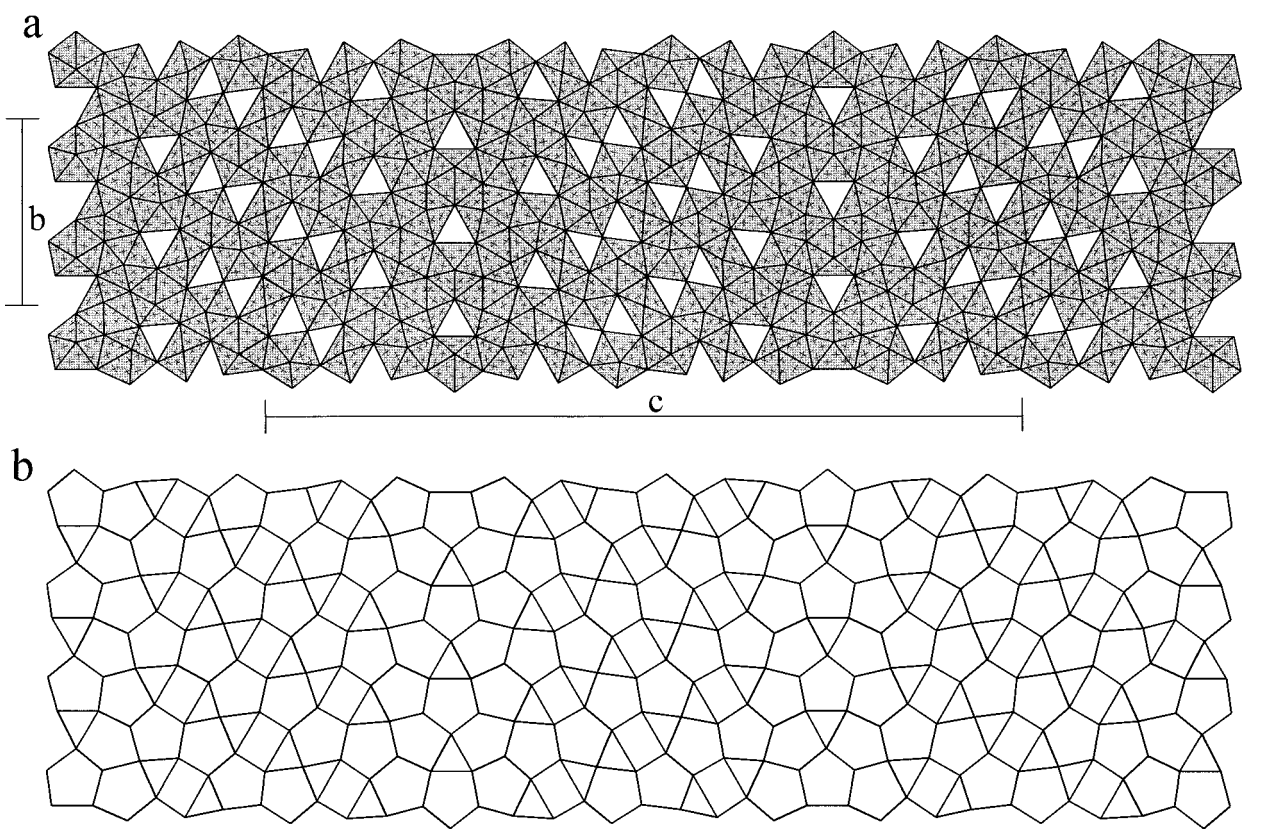

FIGURE 4. The sheet of uranyl polyhedra that occurs in the structure of wölsendorfite projected onto (100). (**a**) polyhedral representation of the sheet, (**b**) sheet anion-topology. The uranyl polyhedra are shaded with crosses.

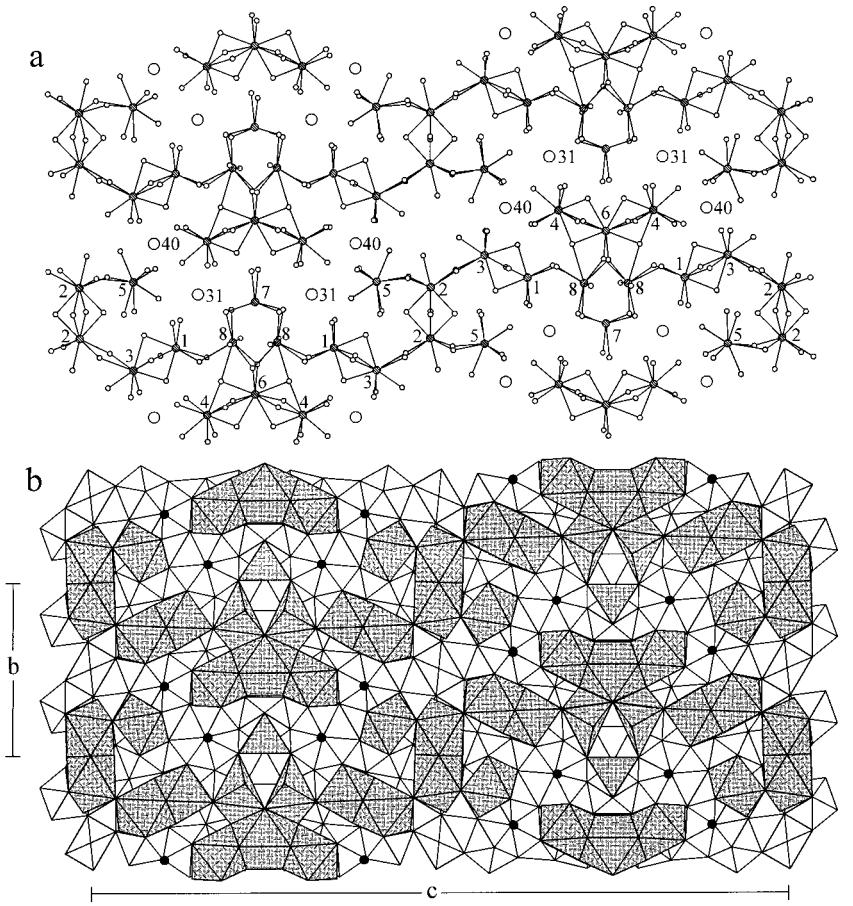

FIGURE 5. The interlayer connectivity in the structure of wölsendorfite projected onto (100). (**a**) ball-and-stick representation, (**b**) polyhedral representation. In (**a**) the Pb^{2+} cations are shown as circles shaded with parallel lines, anions that are bonded to the Pb^{2+} cations are shown as small circles, and H_2O groups that are held in the structure by H bonding only are shown as larger circles. The Pb^{2+} cations and H-bonded H_2O groups are numbered according to Table 3.

49.3 Pb and 2.9 Ba. The bond-valence sums permit the identification of $(OH)^-$ and H_2O groups (Table 7), and the unit cell contains 376 O atoms, 32 $(OH)^-$ groups, and 96 H_2O groups. The bond-valence sums incident upon the O3, O4, and O24 sites are ~1.5 v.u., a value that is intermediate between the expected values for O and $(OH)^-$. However, each of these atoms are part of uranyl ions; $(OH)^-$ groups are not known to occur in uranyl ions, leading to the conclusion that the O3, O4, and O24 atoms are O, despite the low bond-valence sum incident upon the sites. The formula for the wölsendorfite crystal studied can be written as $Pb_{6.16}Ba_{0.36}[(UO_2)_{14}O_{19}(OH)_4](H_2O)_{12}$, with $Z = 8$. This formula has a net charge of –0.96, indicating that there may be minor substitution of monovalent cations at the interlayer sites, although none were detected by chemical analysis, or that the refined site occupancy factors are slightly in error. The formula derived from the microprobe analysis, with H_2O assumed on the basis of the structure determination, is $Pb_{6.10}Ba_{0.36}[(UO_2)_{14}O_{19}(OH)_4](H_2O)_{12}$.

Sheets of uranyl polyhedra

The $Ur\phi_4$ square bipyramids and $Ur\phi_5$ pentagonal bipyramids share equatorial edges and corners to form complex sheets that

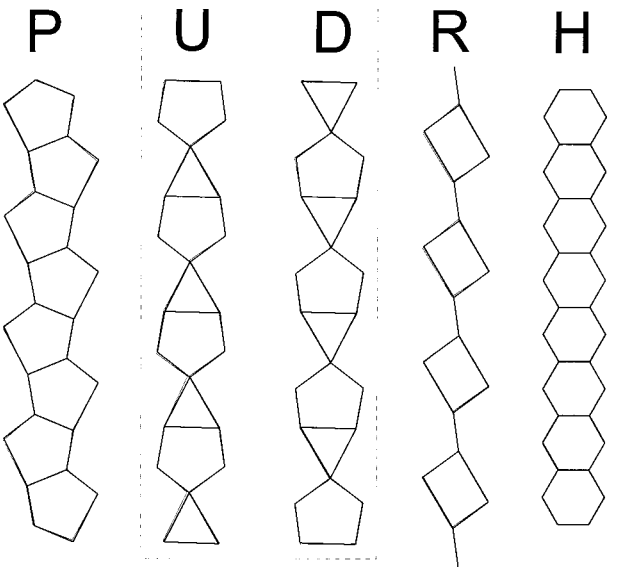

FIGURE 6. Chains of polygons that are required to construct sheet anion-topologies as chain-stacking sequences. After Miller et al. (1996).

are parallel to (100) (Fig. 4). Sheets of uranyl polyhedra are dominant structural features in uranium minerals, but the wölsendorfite sheet is more complex than any other known sheet of uranyl polyhedra, either in a mineral or a synthetic compound. The *c* unit-cell dimension of 55.969 Å is the longest primitive repeat distance of any sheet of uranyl polyhedra. The anion topology of the wölsendorfite sheet, derived using the method of Burns et al. (1996), is shown in Figure 4b. Sheet anion-topologies are two-dimensional tessellations, and the wölsendorfite anion-topology contains triangles, squares and pentagons, as is often the case for the anion topologies of sheets of uranyl polyhedra (Burns et al. 1996).

Interlayer connectivity

The interlayer at $x = 0$ is shown projected along [100] in Figure 5. The interlayer contains the eight symmetrically distinct $Pb\phi_n$ polyhedra, as well as two symmetrically distinct H_2O groups that are held in the structure by H bonding only. The $Pb\phi_n$ polyhedra are polymerized by the sharing of corners, edges, and faces, forming complex infinite heteropolyhedral chains that are parallel to [001] (Fig. 5).

Comparison to related structures

The wölsendorfite sheet is an example of structural complexity that challenges our understanding of mineral structures. The vandendriesscheite sheet (Fig. 1i) is also very complex, but its primitive *b* unit-cell dimension of 41.378 Å (Burns 1997) is short compared to $c = 55.969$ Å in the wölsendorfite sheet. The sheets of uranyl polyhedra that occur in other lead uranyl oxide hydrates (Fig. 1) are topologically simpler than either the wölsendorfite or vandendriesscheite sheets. As is the case in the wölsendorfite sheet, both the sayrite (Fig. 1d) and curite (Fig. 1a) sheets contain both $Ur\phi_4$ and $Ur\phi_5$ polyhedra, whereas the fourmarierite, richetite, and vandendriesscheite sheets contain only $Ur\phi_5$ pentagonal bipyramids.

Miller et al. (1996) discussed the characterization of sheet anion-topologies as stacking sequences of chains, and this approach was successfully applied to the vandendriesscheite anion-topology by Burns (1997). If consideration is restricted to those sheets that contain only uranyl polyhedra that occur in minerals and synthetic phases (with the exception of the curite anion-topology), only four chains of polygons (Fig. 6) are required to construct all of the anion topologies. The **P** and **H** chains involve edge-sharing pentagons and hexagons, respectively. The arrowhead chains involve the sharing of an edge between a pentagon and a triangle, with the other corner of the triangle shared with the next pentagon in the chain. The arrowhead chain has a directional aspect, and may point either up (**U**) or down (**D**). The **R** chain consists of rhombs connected by lines. Various rules on how these chains fit together to form sheet anion-topologies were identified by Miller et al. (1996).

First consider the relatively simple α-U_3O_8 and β-U_3O_8 anion-topologies shown in Figure 7. The α-U_3O_8 anion-topology (also sometimes referred to as the protasite anion-topology) is the basis for the sheets that occur in the structures of protasite, richetite, becquerelite, billietite, and compreignacite, as well

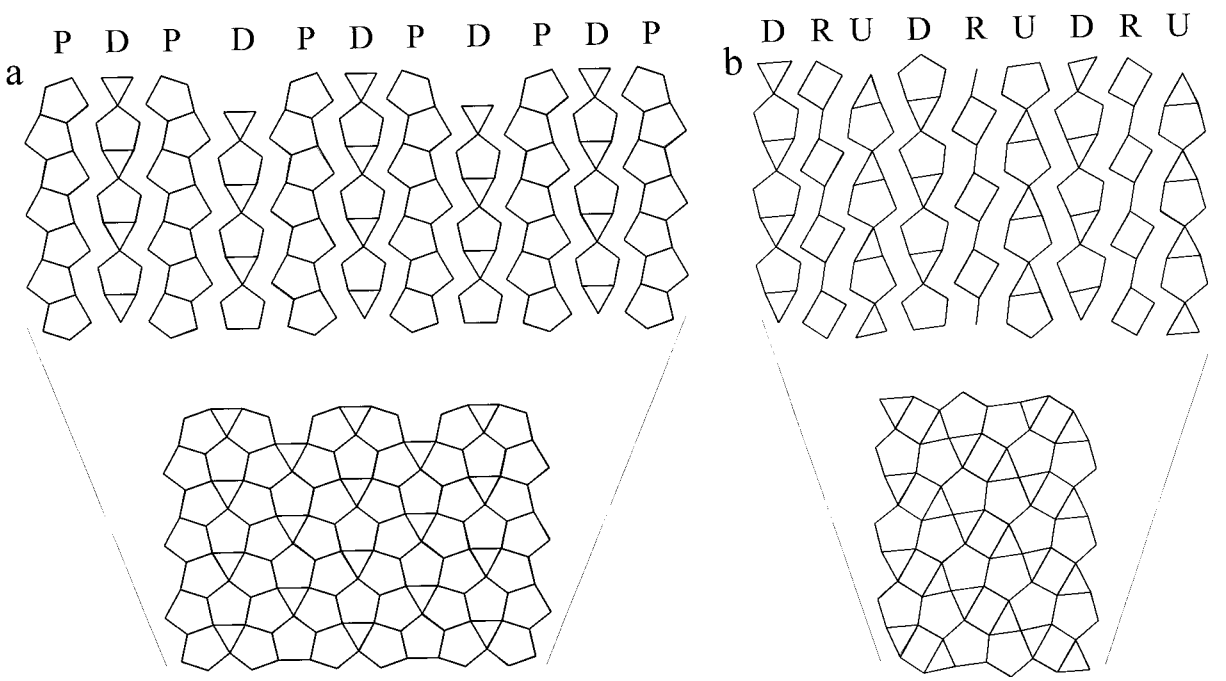

FIGURE 7. The generation of sheet anion-topologies as chain-stacking sequences. (**a**) the α-U_3O_8 anion-topology, (**b**) the β-U_3O_8 anion-topology.

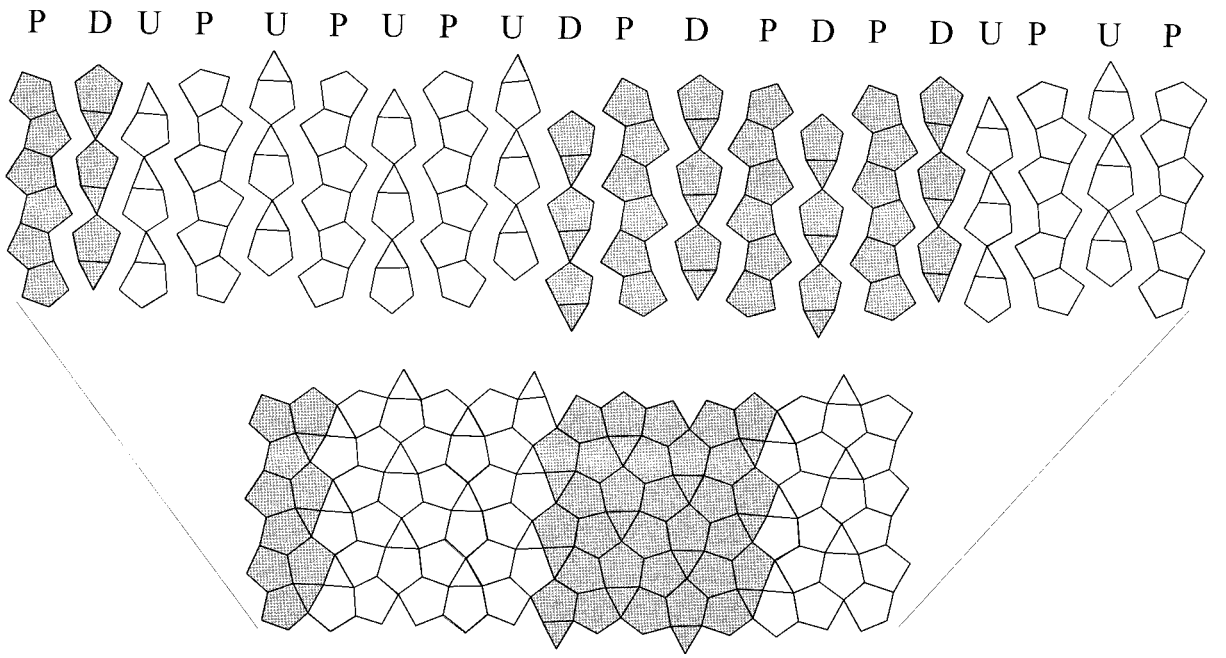

FIGURE 8. Generation of the vandendriesscheite anion-topology using a chain-stacking sequence.

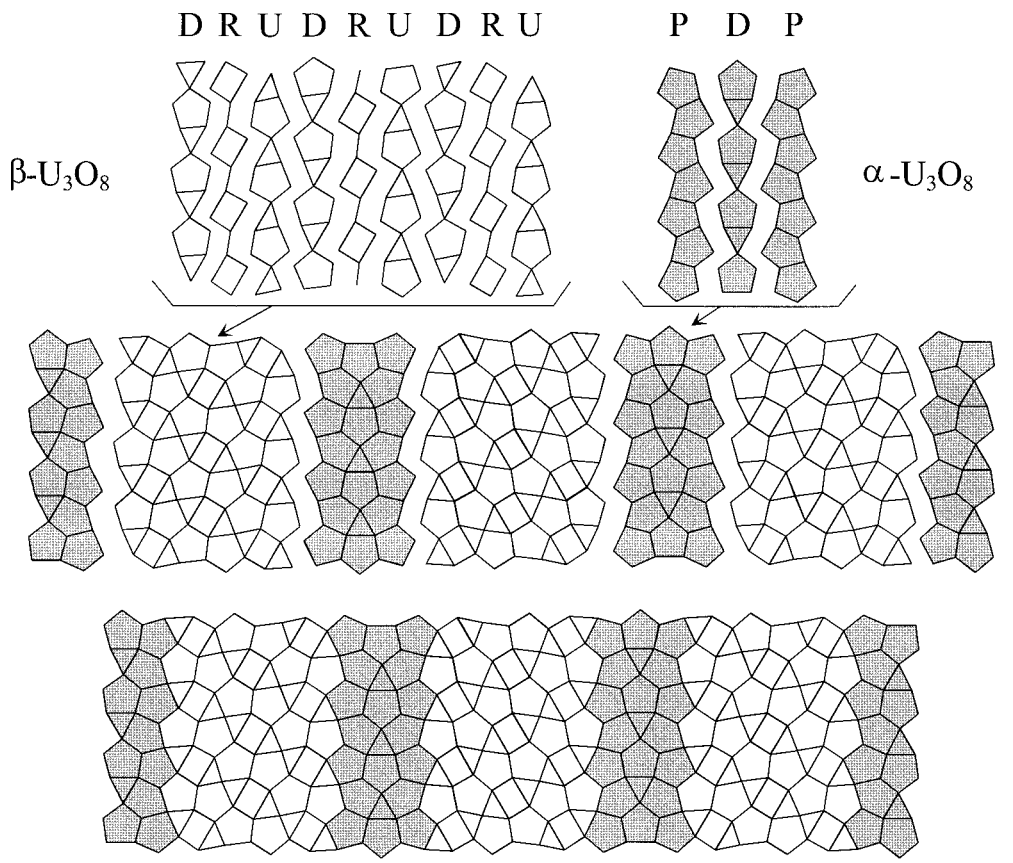

FIGURE 9. Generation of the wölsendorfite anion-topology using a chain-stacking sequence. The α-U_3O_8 component of the anion-topology is shaded.

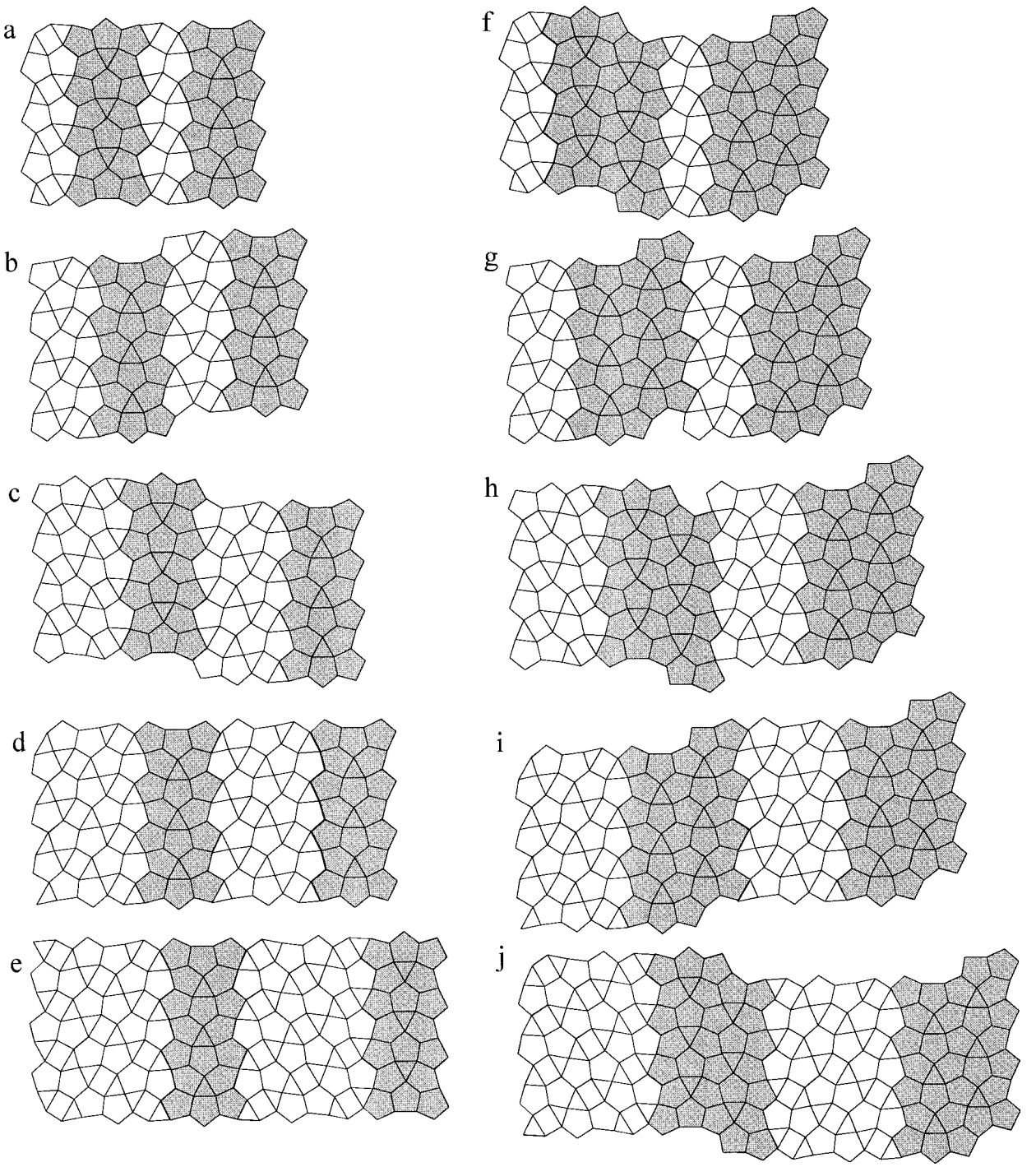

FIGURE 10. Various hypothetical sheet anion-topologies obtained by combining slabs of the α-U_3O_8 and β-U_3O_8 anion-topologies. The α-U_3O_8 component of the anion-topology is shaded. Only (**e**) is known from a mineral structure.

as in the mixed-valence α-U_3O_8 phase. The β-U_3O_8 anion-topology is less common; it is only known from the structure of ianthinite and the mixed-valence β-U_3O_8 phase. The generation of each of these anion topologies using chain-stacking sequences is illustrated in Figure 7. The α-U_3O_8 anion-topology can be constructed using only the **P** and **U** or **D** chains, with the repeat sequence **PUPU**… The β-U_3O_8 anion-topology requires the use of the **P**, **D,** and **R** chains, with the repeat sequence **DRUDRU**…

The complex vandendriesscheite anion-topology can be derived as a chain-stacking sequence (Fig. 8) using the **P**, **D,** and **U** chains, with the sequence **PDUPUPUPUPDPDPDPDUPUPU**… (Burns 1997). Note that the sequences **UPUP**… and **DPDP**… in the vandendriesscheite anion-topology are identical to the α-U_3O_8 anion-topology sequence, and the vandendriesscheite anion-topology can be assembled using slabs of α-U_3O_8 anion-topology that alternate up and down.

The wölsendorfite anion-topology is generated using a chain-stacking sequence with the **R**, **D**, **P**, and **U** chains, resulting in a complex repeat sequence (Fig. 9). The repeat sequence involves the strings **DRUDRUDRU** and **PDP** (Fig. 9), which are slabs of the β-U_3O_8 and α-U_3O_8 anion-topologies, respectively. Thus, the wölsendorfite anion-topology may be assembled using slabs of the α-U_3O_8 and β-U_3O_8 anion-topologies, and it follows that the wölsendorfite sheet is structurally intermediate between the α-U_3O_8 and β-U_3O_8-type sheets.

As was the case with the sheets of uranyl polyhedra, the interlayer contained in the structure of wölsendorfite is more complex than the interlayers in most uranyl minerals. The interlayers of lead uranyl oxide hydrate minerals display a range of polymerization. The $Pb\phi_8$ polyhedra in the interlayer of sayrite are not polymerized, and only half of the $Pb\phi_n$ polyhedra in the interlayer of vandendriesscheite share polyhedral elements with other $Pb\phi_n$ polyhedra to form dimers. The fourmarierite interlayer contains dimers of edge-sharing polyhedra only. The richetite interlayer is very complex, with clusters of partially occupied $Pb\phi_n$ polyhedra that share faces and edges, as well as sharing polyhedral elements with $M^{2+}\phi_6$ octahedra. The curite interlayer involves chains of face-sharing $Pb\phi_n$ polyhedra that are two polyhedra wide, but they do not resemble the chains found in the interlayer of wölsendorfite. Thus, the complex chains of polymerized polyhedra (Fig. 5) in the wölsendorfite interlayer are unusual in both their complexity and degree of polymerization.

DISCUSSION

It is well known that uranyl minerals possess fascinatingly diverse structures, but a new level of structural complexity in uranyl minerals was revealed by the wölsendorfite sheet. The sheet illustrates well the usefulness of the sheet anion-topology approach for the classification and comparison of the structures of uranyl minerals. Using this approach, it is readily apparent that the sheet contains slabs of simpler, previously known sheets.

Why do the uranyl polyhedra in wölsendorfite adopt such a complex configuration? Is it likely that similarly complex sheets of uranyl polyhedra with different configurations exist in other minerals? It is impossible to provide answers to either of these questions at this time; considerable research into the energetics of these sheets, and into the structures of uranyl minerals, is essential to gain an understanding of the crystal-chemical principles that result in such complex sheets. However, it is apparent that there are many anion topologies and corresponding sheets that appear to be chemically feasible but that have not been observed in any structure. Consider, for example, sheet anion-topologies developed using slabs of various widths of the α-U_3O_8 and β-U_3O_8 anion topologies; a few of the possible combinations are shown in Figure 10. Of these, only one is known from a structure (e), despite the fact that the topologies are each complete tilings of two-dimensional space. We currently do not have a means to discriminate which of these is energetically favorable.

ACKNOWLEDGMENTS

The crystal used in this study was provided by the Canadian Museum of Nature. Robert A. Gault of the Canadian Museum of Nature carried out the electron microprobe analysis of the crystals of wölsendorfite. This research was funded by the National Science Foundation (EAR98-04723).

REFERENCES CITED

Beddoe-Stephens, B. and Secher, K. (1982) Barian wölsendorfite from east Greenland. Mineralogical Magazine, 46, 130–132.

Belov, L.N. and Fedorov, O.V. (1974) New data on wölsendorfite. Zapiski Vsesoyuznogo Mineralogicheskogo Obshchestva, 103, 718–719 (in Russian).

Brese, N.E. and O'Keeffe, M. (1991) Bond-valence parameters for solids. Acta Crystallographica, B47, 192–197.

Burns, P.C. (1997) A new uranyl oxide hydrate sheet in the structure of vandendriesscheite: Implications for mineral paragenesis and the corrosion of spent nuclear fuel. American Mineralogist, 82, 1176–1186.

———(1998a) The structure of richetite, a rare lead uranyl oxide hydrate. Canadian Mineralogist, 36, 187–199.

———(1998b) Implications of solid-solution in the structure of boltwoodite. Canadian Mineralogist, 36, 1069–1075.

———(1998c) The structure of compreignacite, $K_2[(UO_2)_3O_2(OH)_3]_2(H_2O)_7$. Canadian Mineralogist, 36, 1061–1067.

———(1998d) CCD area detectors of X-rays applied to the analysis of mineral structures. Canadian Mineralogist, 36, 847–853.

———(1999) Cs boltwoodite obtained by ion exchange from single crystals: Implications for radionuclide release in a nuclear repository. Journal of Nuclear Materials, 265, 218–223.

Burns, P.C. and Hill, F.C. (1999) Implications of the synthesis and structure of the Sr analogue of curite. Canadian Mineralogist, in press.

Burns, P.C., Miller, M.L., and Ewing, R.C. (1996) U^{6+} minerals and inorganic phases: a comparison and hierarchy of crystal structures. Canadian Mineralogist, 34, 845–880.

Burns, P.C., Ewing, R.C., and Hawthorne, F.C. (1997a) The crystal chemistry of hexavalent uranium: Polyhedral geometries, bond-valence parameters, and polyhedral polymerization. Canadian Mineralogist, 35, 1551–1570.

Burns, P.C., Ewing, R.C., and Miller, M.L. (1997b) Incorporation mechanisms of actinide elements into the structures of U^{6+} phases formed during the oxidation of spent nuclear fuel. Journal of Nuclear Materials, 245, 1–9.

Burns, P.C., Finch, R.J., Hawthorne, F.C., Miller, M.L., and Ewing, R.C. (1997c) The crystal structure of ianthinite, $[U^{4+}_2(UO_2)_4O_6(OH)_4(H_2O)_4](H_2O)_5$: A possible phase for Pu^{4+} incorporation during the oxidation of spent nuclear fuel. Journal of Nuclear Materials, 249, 199–206.

Evans, H.T., Jr. (1963) Uranyl ion coordination. Science, 141, 154–157.

Finch, R.J. and Ewing, R.C. (1992) The corrosion of uraninite under oxidizing conditions. Journal of Nuclear Materials, 190, 133–156.

Finch, R.J., Miller, M.L., and Ewing, R.C. (1992) Weathering of natural uranyl oxide hydrates: schoepite polytypes and dehydration effects. Radiochimica Acta, 58/59, 433–443.

Finch, R.J., Cooper, M.A., Hawthorne, F.C., and Ewing, R.C. (1996) The crystal structure of schoepite, $[(UO_2)_8O_2(OH)_{12}](H_2O)_{12}$. Canadian Mineralogist, 34, 1071–1088.

Finch, R.J., Hawthorne, F.C., and Ewing, R.C. (1998) Structural relations among schoepite, metaschoepite and "dehydrated schoepite". Canadian Mineralogist, 36, 831–845.

Finn, P.A., Hoh, J.C., Wolf, S.F., Slater, S.A., and Bates, J.K. (1996) The release of uranium, plutonium, cesium, strontium, technetium and iodine from spent fuel under unsaturated conditions. Radiochimica Acta, 74, 65–71.

Fleischer, M. and Mandarino, J.A. (1995) Glossary of mineral species. The Miner-

alogical Record Inc., Tucson, Arizona.
Frondel, C. (1958) Systematic mineralogy of uranium and thorium. U.S. Geological Survey Bulletin 1064.
Ibers, J.A. and Hamilton, W.C., eds. (1974) International Tables for X-ray Crystallography, volume IV. The Kynoch Press, Birmingham, U.K.
Kovba, L.M. (1972) Crystal structure of $K_2U_7O_{22}$. Journal of Structural Chemistry, 13, 235–238.
Miller, M.L., Finch, R.J., Burns, P.C., and Ewing, R.C. (1996) Description and classification of uranium oxide hydrate sheet topologies. Journal of Materials Research, 11, 3048–3056.
Murakami, T., Ohnuki, T., Isobe, H., and Sato, T. (1997) Mobility of uranium during weathering. American Mineralogist, 82, 888–899.
Pagoaga, M.K., Appleman, D.E., and Stewart, J.M. (1987) Crystal structures and crystal chemistry of the uranyl oxide hydrates becquerelite, billietite, and protasite. American Mineralogist, 72, 1230–1238.
Piret, P. (1985) Structure cristalline de la fourmariérite, $Pb(UO_2)_4O_3(OH)_4.4H_2O$. Bulletin de Minéralogie, 108, 659–665.
Piret, P., Deliens, M., Piret-Meunier, J., and Germain, G. (1983) La sayrite, $Pb_2[(UO_2)_5O_6(OH)_2]\0 4H_2O$, nouveau minéral; propriétés et structure cristalline. Bulletin de Minéralogie, 106, 299–304.
Protas, J. (1957) La wölsendorfite, nouvelle espèce uranifere. Compte Rendus, 244, 2942
Sowder, A.G., Clark, S.B., and Fjeld, R.A. (1996) The effect of silica and phosphate on the transformation of schoepite to becquerelite and other uranyl phases. Radiochimica Acta, 74, 45–49.
Taylor, J.C., Stuart, W.L., and Mumme, I.A. (1981) The crystal structure of curite. Journal of Inorganic and Nuclear Chemistry, 43, 2419–2423.
Toussaint, J. (1961) Sur la structure de la wölsendorfite de Shinkolobwe. Annales Sociéte Géologique de Belgique, 84, 365–373.
Vochten, R. and van Haverbeke, L. (1990) Transformation of schoepite into the uranyl oxide hydrates; becquerelite, billietite and wölsendorfite. Mineralogy and Petrology, 43, 65–72.
Vochten, R., van Haverbeke, L., Van Springel, K., and De Grave, E. (1995) Soddyite: Synthesis under elevated-temperature and pressure, and study of some physicochemical characteristics. Neues Jahrbuch für Mineralogie. Monatshefte, 10, 470–480.
Vochten, R., Blaton, N., Peeters, O., Van Springel, K., and Van Haverbeke, L. (1997) A new method of synthesis of boltwoodite and of formation of sodium boltwoodite, uranophane, sklodowskite and kasolite from boltwoodite. Canadian Mineralogist, 35, 735–741.
Wronkiewicz, D.J., Bates, J.K., Wolf, S.F., and Buck, E.C. (1996) Ten-year results from unsaturated drip tests with UO_2 at 90°C: implications for the corrosion of spent nuclear fuel. Journal of Nuclear Materials, 238, 78–95.

MANUSCRIPT RECEIVED DECEMBER 7, 1999
MANUSCRIPT ACCEPTED JULY 6, 1999
PAPER HANDLED BY RODNEY C. EWING